THE ROYAL SOCIETY

Direct numerical simulation of premixed turbulent flames

By Stewart Cant

CFD Laboratory, Department of Engineering, University of Cambridge, Trumpington Street, Cambridge CB2 1PZ, UK

The enormous increase in computer power during the recent past has made it possible for the first time to carry out direct numerical simulation (DNS) of turbulent reacting flow fields, without the use of a turbulence model. This has opened up a significant new area of research into the fundamental processes of flame–turbulence interaction since it is now possible to solve the governing equations in full detail, resolving even the smallest of the important features of the flow and the flame. In many ways, the technology of DNS remains in its infancy, and the present work seeks to extend current methods in order to take advantage of massively parallel supercomputers. The governing equations are presented and necessary simplifications are justified in the light of current computational capabilities. A numerical discretization scheme suitable for parallel implementation is described, and results are presented for a series of simulations of simple test problems. The relevance of the results is discussed in the light of current turbulent-combustion modelling, and suggestions are made for future work.

Keywords: combustion; turbulence; modelling; premixed flames

1. Introduction

Combustion in practical systems, such as gas turbines, reciprocating engines and industrial boilers, almost invariably takes place in a turbulent-flow field. In many cases, the turbulence is deliberately enhanced in order to improve mixing rates and maximize the rate of reaction, while in other cases, the turbulence is simply a natural consequence of the geometry and the conditions of the system together with those of the surrounding environment. It is necessary in all cases to have some understanding of the interaction of the turbulent-flow field with the flame in order to help control the rate of heat release, the temperature distribution within the system and the rate of formation of unwanted emissions such as CO, NO_x and particulates.

Unfortunately, the mathematical treatment of turbulence is not sufficiently developed to enable closed-form solutions to be obtained, even for relatively simple problems. By contrast, the phenomenology of turbulence is fairly well developed and has led to a number of modelling approaches that are suitable for use in the context of computational fluid dynamics (CFD) for quite complex flows. CFD is now widely used in many industries as part of the design process, despite evidence that the predictive capability of many standard turbulence models is limited to the class of flows for which they were validated. The extension of CFD-based modelling to combustion systems is not straightforward due to the added complexities of chemistry and

heat release, which, in general, must also be modelled, and success in this field has been far from universal. For many industries, the potential cost savings of CFD as compared with traditional prototype testing are very large, and there remains an urgent need for better physical models. This in turn calls for reliable statistical data for the validation of existing turbulence and turbulent-combustion models, and for the development of new modelling concepts. The most obvious source of such data is experiment, and recent developments in laser-based diagnostic techniques have allowed simultaneous two-dimensional imaging of velocity and scalar fields to a very high level of detail. The availability of such data is extremely useful in model development, but the physical processes of turbulent combustion are fully three dimensional and time dependent and so the picture remains incomplete.

At the same time, recent advances in computer power have made it possible for the first time to consider direct numerical simulation (DNS) of turbulent reacting flow. Following the pioneering work of Riley *et al.* (1986) in non-premixed combustion, and of Rutland *et al.* (1990) in the premixed case, it has become possible to simulate, in full detail, without any kind of turbulence modelling, the three-dimensional and time-evolving flow field in a number of simple combustion problems. Naturally, there is a cost. The absence of turbulence modelling imposes the absolute requirement that every scale of the turbulent motion be resolved in both space and time. In the presence of a flame, the smallest scales may well be those of the reaction and diffusion processes that give the flame its structure, and they too must be resolved. The precise number of numerical grid points required to achieve adequate physical resolution also depends on the nature of the spatial discretization scheme in use, while the size of the problem itself is set by the size and power of the largest available computer. It can be shown that the storage requirement scales as the Reynolds number raised to the power 9/4, while the computing effort scales as the Reynolds number raised to a power of between 3 and 4 depending on the particular time-advancement scheme in use. These scaling laws remain true even where the resolution requirement is set by the flame rather than the smallest scales of the turbulence, since the thermal thickness of the flame may be expressed as a fraction of the Kolmogorov length-scale. Thus, the need for additional resolution at small scale in order to capture complex chemical or diffusive structure simply acts as a multiplier on the overall storage requirement. The introduction of complex chemistry is particularly expensive due to the need to store additional scalar variables, which, in general, will all require high resolution. In view of the stiffness introduced by many detailed chemical reaction schemes, the penalty in terms of computing effort can be especially severe.

In terms of numerical methods, the major challenge is to find a spatial discretization scheme that resolves adequately the high-wavenumber components of the solution without incurring unacceptable computational costs. Fourier spectral methods are particularly suitable in this regard, but bring severe restrictions on problem formulation due to the need for periodic boundary conditions. Much of the progress that has been made in combustion DNS has been based on the use of high-accuracy finite-difference methods (Lele 1992), which allow complete flexibility in the specification of boundary conditions, for minimal loss of accuracy relative to spectral methods. Another major contribution has been the development of a general formulation for Navier–Stokes boundary conditions (Poinsot & Lele 1992) based on analysis of characteristics, and this has been extended to handle combustion problems with complex chemistry (Baum *et al.* 1998). Several combustion DNS studies have been carried

out with objectives specifically related to modelling (Cant *et al.* 1990; Rutland & Cant 1994; Alshaalan & Rutland 1998) and improvements to modelling practice have followed (Bray & Cant 1991; Zhang & Rutland 1995). Other studies have focused on the flame–turbulence interaction process at the fundamental level (Kollman & Chen 1998; Echekki & Chen 1996). The field is growing steadily and recent reviews (Poinsot *et al.* 1995; Vervisch & Poinsot 1998) provide a useful overview of the current state of the art. Clearly, the usefulness of DNS results generally depends, to a significant extent, on achieving a Reynolds number that is as high as possible, and, ideally, is comparable with the turbulence Reynolds numbers of practical systems. Despite all of the improvements in the technology of combustion DNS, this goal is not yet within reach.

The advent of massively parallel computers is now providing a new impetus to DNS by offering the possibility for problem size, and, hence, Reynolds number, to be significantly increased. Algorithm design for the effective use of parallel computers has become a major research topic in itself, and it is clear that transfer of existing codes to parallel architectures is not necessarily the most effective approach. The present work is concerned both with obtaining physically relevant results from combustion DNS and with gaining experience in the development and use of DNS codes on massively parallel computers. An example of the design compromises that have been made is in the use of second-order numerical schemes. It is recognized that the accuracy and resolving power of second-order schemes is limited by comparison with spectral or other high-order methods, and that more grid points will be necessary to achieve the same degree of resolution. The advantage is that a simple second-order scheme is straightforward to implement using a parallel domain-decomposition strategy and is extremely efficient in execution (Bushe *et al.* 1997; Bushe & Cant 1996).

The present paper is intended to describe recent work in DNS of premixed turbulent combustion, carried out to investigate basic flame–turbulence interactions and to provide statistical data in support of modelling efforts. The governing equations are presented and necessary simplifications are discussed. The numerical discretization and solution schemes are described and their parallel implementation is outlined. A set of test problems is presented together with the procedure for obtaining solutions. Results of interest in the modelling of turbulent flames are shown and the implications are discussed in terms of modelling and of future simulation efforts.

2. Governing equations

The equations governing the flow of a compressible reacting gas may be stated in Cartesian tensor notation as

$$\frac{\partial}{\partial t}\rho + \frac{\partial}{\partial x_k}\rho u_k = 0, \tag{2.1}$$

$$\frac{\partial}{\partial t}\rho u_i + \frac{\partial}{\partial x_k}\rho u_k u_i = -\frac{\partial}{\partial x_i}P + \frac{\partial}{\partial x_k}\tau_{ki}, \tag{2.2}$$

$$\frac{\partial}{\partial t}\rho E + \frac{\partial}{\partial x_k}\rho u_k E = -\frac{\partial}{\partial x_k}u_k P + \frac{\partial}{\partial x_i}u_k\tau_{ki} - \frac{\partial}{\partial x_k}q_k, \tag{2.3}$$

$$\frac{\partial}{\partial t}\rho Y_\alpha + \frac{\partial}{\partial x_k}\rho u_k Y_\alpha = w_\alpha - \frac{\partial}{\partial x_k}\rho V_{\alpha k} Y_\alpha, \quad \alpha = 1, \ldots, N, \tag{2.4}$$

where ρ is the density, u_i is the velocity vector, P is the pressure, E is the stagnation internal energy, and Y_α is the mass fraction of species α in the reacting mixture that contains N species in total. The viscous stress tensor τ_{ki} is given by

$$\tau_{ki} = \mu\left(\frac{\partial u_k}{\partial x_i} + \frac{\partial u_i}{\partial x_k}\right) - \tfrac{2}{3}\mu\frac{\partial u_m}{\partial x_m}\delta_{ki}, \tag{2.5}$$

where μ is the viscosity, and the heat flux vector q_k is given by

$$q_k = -\lambda\frac{\partial T}{\partial x_k} + \rho\sum_{\alpha=1}^{N} h_\alpha V_{\alpha k} Y_\alpha,$$

where λ is the thermal conductivity, T is the temperature, h_α is the enthalpy of species α, and $V_{\alpha k}$ is the diffusion velocity of species α relative to the mixture. The chemical reaction rate for species α is given by

$$w_\alpha = W_\alpha \sum_{m=1}^{M}\left[(\nu''_{\alpha,m} - \nu'_{\alpha,m})A_m T^{n_m}\exp\left(-\frac{E_m}{R^0 T}\right)\prod_{\beta=1}^{N}\left(\frac{\rho Y_\beta}{W_\beta}\right)^{\nu'_{\beta,m}}\right],$$

for a reaction mechanism involving N species and M steps, where W_α is the molar mass of species α and R_0 is the universal gas constant. For step m, $\nu'_{\alpha,m}$ and $\nu''_{\alpha,m}$ are, respectively, the reactant and product stoichiometric coefficients, while A_m, n_m and E_m are, respectively, the frequency factor, temperature exponent and activation energy. The compatibility condition on the species mass fractions is

$$\sum_{\alpha=1}^{N} Y_\alpha = 1.$$

The thermal equation of state is

$$P = \rho R^0 T\sum_{\alpha=1}^{N}\frac{Y_\alpha}{W_\alpha},$$

and the caloric equation of state is

$$E = C_{\mathrm{V}}T + \tfrac{1}{2}u_k u_k + \sum_{\alpha=1}^{N} h^0_\alpha Y_\alpha,$$

where C_{V} is the mixture specific heat capacity at constant volume and h^0_α is the enthalpy of formation of species α.

In order to make the governing equations tractable even for DNS, it is necessary to introduce some simplifications. The computational cost of resolving both the turbulence and the chemistry in three dimensions is simply too great for present-day computers and a compromise must be made. If a comprehensive chemical treatment is required, then the problem must be reduced to two dimensions, with the loss of important dynamical information about the turbulent field. For present purposes, the turbulent-flow field is regarded as paramount and its representation in three dimensions must take precedence over a detailed representation of the chemistry. Thus, while the simulation of the turbulence is indeed direct, the chemical

treatment is reduced to a minimum necessary to capture the basic features of the flame–turbulence interaction.

To this end, a one-step irreversible reaction is assumed

$$\mathrm{R} \rightarrow \mathrm{P},$$

and a reaction-progress variable is defined based on the mass fraction of the product species

$$c = \frac{Y_{\mathrm{P}} - Y_{\mathrm{P0}}}{Y_{\mathrm{P}\infty} - Y_{\mathrm{P0}}}.$$

The reaction rate for the one-step reaction is governed by a simplified Arrhenius rate law

$$w = B\rho(1-c)\exp\left(-\frac{E}{R^0 T}\right),$$

where B is the pre-exponential factor and E is the activation energy. In addition, a Fickian diffusion law is assumed to be applicable,

$$\rho V_{ck} c = -\rho D \frac{\partial c}{\partial x_k},$$

where the single diffusion coefficient D is a known function of the local thermochemical state. The purpose of the simplified chemical treatment is to enable the replacement of the $N-1$ conservation equations for the species mass fraction equations by a single conservation equation for the reaction-progress variable:

$$\frac{\partial}{\partial t}\rho c + \frac{\partial}{\partial x_k}\rho u_k c = w + \frac{\partial}{\partial x_k}\rho D \frac{\partial c}{\partial x_k}. \tag{2.6}$$

The simplified form of the equations of state are

$$P = \rho R T, \tag{2.7}$$

$$E = C_{\mathrm{V}} T + \tfrac{1}{2} u_k u_k + H(1-c), \tag{2.8}$$

where H is the heat of reaction per unit mass of reactants consumed. The heat flux vector simplifies to

$$q_k = -\lambda \frac{\partial T}{\partial x_k} - \frac{\partial}{\partial x_k}\rho D H \frac{\partial c}{\partial x_k}.$$

The equations are non-dimensionalized using a set of standard values of the principal variables, namely u_0, l_0, $t_0 = l_0/u_0$, ρ_0 and T_0. In addition, standard values of the transport coefficients μ_0, λ_0, D_0 and C_{V0} are chosen. The normalizing pressure P_0 is chosen to be representative of dynamic rather than thermochemical effects and the relation $P_0 = \rho_0 u_0^2$ is employed. The temperature is non-dimensionalized according to

$$T = \frac{\hat{T} - T_0}{T_{\mathrm{ad}} - T_0},$$

where $\hat{T}$ denotes the instantaneous dimensional value, T_0 is the initial temperature, and T_{ad} is the adiabatic flame temperature, given by $T_{\mathrm{ad}} = T_0 + H/C_{\mathrm{P0}}$. This form makes the non-dimensional temperature lie between zero and unity for adiabatic

combustion, but these bounds may be exceeded due to other effects such as compression or external heating. The internal energy is non-dimensionalized with respect to $C_{\mathrm{P}0}T_0$.

With all variables now assumed to be in non-dimensional form, the governing equations become

$$\frac{\partial}{\partial t}\rho + \frac{\partial}{\partial x_k}\rho u_k = 0, \tag{2.9}$$

$$\frac{\partial}{\partial t}\rho u_i + \frac{\partial}{\partial x_k}\rho u_k u_i = -\frac{\partial}{\partial x_i}P + \frac{1}{Re}\frac{\partial}{\partial x_k}\tau_{ki}, \tag{2.10}$$

$$\frac{\partial}{\partial t}\rho E + \frac{\partial}{\partial x_k}\rho u_k E = -(\gamma-1)\mathcal{M}^2\frac{\partial}{\partial x_k}u_k P + (\gamma-1)\frac{\mathcal{M}^2}{Re}\frac{\partial}{\partial x_i}u_k\tau_{ki} + \frac{\tau_{\mathrm{H}}}{RePr}\frac{\partial}{\partial x_k}\lambda\frac{\partial T}{\partial x_k} + \frac{\tau_{\mathrm{H}}}{ReSc}\frac{\partial}{\partial x_k}\rho D\frac{\partial c}{\partial x_k}, \tag{2.11}$$

$$\frac{\partial}{\partial t}\rho c + \frac{\partial}{\partial x_k}\rho u_k c = w + \frac{1}{ReSc}\frac{\partial}{\partial x_k}\rho D\frac{\partial c}{\partial x_k}, \tag{2.12}$$

where the viscous stress tensor τ_{ki} remains unchanged in form from (2.5), and the chemical reaction rate is given by

$$w = B^*\rho(1-c)\exp\left(-\frac{\beta(1-T)}{1-\alpha(1-T)}\right).$$

The non-dimensional equations of state are

$$P = \frac{1}{\gamma\mathcal{M}^2}\rho(1+\tau_{\mathrm{H}}T), \tag{2.13}$$

$$E = \frac{1}{\tau_{\mathrm{H}}}(1+\tau_{\mathrm{H}}T) + \tfrac{1}{2}(\gamma-1)\mathcal{M}^2 u_k u_k + \tau_{\mathrm{H}}(1-c). \tag{2.14}$$

The main non-dimensional parameters appearing in these equations are the Reynolds number Re, the Prandtl number Pr, the Schmidt number Sc, and the Mach number $\mathcal{M}$, defined, respectively, by

$$Re = \frac{\rho_0 u_0 l_0}{\mu_0}, \qquad Pr = \frac{\mu_0 C_{\mathrm{P}0}}{\lambda_0}, \qquad Sc = \frac{\mu_0}{\rho_0 D_0}, \qquad \mathcal{M} = \frac{u_0}{a_0},$$

where the speed of sound, a_0, is given by $a_0 = \sqrt{\gamma R T_0}$. The ratio of specific heats γ, the heat release parameters τ_{H} and α, the Zeldovich number β, and the pre-exponential factor B^* are given by

$$\gamma = \frac{C_{\mathrm{P}0}}{C_{\mathrm{V}0}}, \qquad \tau_{\mathrm{H}} = \frac{\alpha}{1-\alpha} = \frac{T_{\mathrm{ad}}-T_0}{T_0},$$
$$\beta = \frac{E(T_{\mathrm{ad}}-T_0)}{R^0 T_{\mathrm{ad}}^2}, \qquad B^* = \frac{B}{\rho_0 u_0}\exp\left(-\frac{\beta}{\alpha}\right).$$

A final level of approximation is introduced by assuming that the Mach number is negligibly small. Substituting the caloric equation of state into the energy equation yields an equation for the temperature in the limit of low Mach number,

$$\frac{\partial}{\partial t}\rho T + \frac{\partial}{\partial x_k}\rho u_k T = \frac{1}{RePr}\frac{\partial}{\partial x_k}\lambda\frac{\partial T}{\partial x_k} + w, \tag{2.15}$$

where C_{V} is assumed constant. The pressure may be split formally into thermochemical and dynamic components leading to the low-Mach-number form of the thermal equation of state:

$$\rho = \frac{1}{1 + \tau_{\mathrm{H}} T}. \tag{2.16}$$

The formulation is completed by choosing values for the key dimensional quantities. The velocity u_0 is set equal to the planar unstrained laminar-flame speed u_l, and the length-scale l_0 is set such that the dimensionless domain size is unity. Then the non-dimensionalizing time-scale t_0 becomes equal to the laminar-flame passage time τ, i.e. the time taken for the laminar flame to pass completely through the computational box. All of the other dimensional quantities, ρ_0, T_0, μ_0, λ_0, D_0 and $C_{\mathrm{V}0}$, are set to values appropriate to the reactant mixture.

3. Discretization

The non-dimensional governing equations are discretized in space using the classical second-order central difference method due to Harlow & Welch (1965). This method has adequate accuracy for a well-resolved combustion DNS, where the small-scale activity is dominated by chemistry and natural diffusion, and the smallest scales of turbulence are an order of magnitude larger than the computational grid spacing. The second-order scheme is simple to implement, is computationally efficient in terms of both CPU time and memory usage, and is easily adapted for use on massively parallel computers. A further advantage is that the scheme naturally conserves kinetic energy as well as momentum. This property is particularly useful in DNS computations and is discussed by Orszag (1969), who gives a proof for the present scheme.

The general form of the conservation equations is given by

$$\frac{\partial \rho\phi}{\partial t} = S_\phi + \frac{\partial}{\partial x_k}\left[\Gamma_\phi \frac{\partial \phi}{\partial x_k} - \rho u_k \phi\right], \tag{3.1}$$

where ϕ is one of u, v, w, T or c, Γ_ϕ is the appropriate diffusivity, and S_ϕ is a generalized source term containing all other terms in the equation for ϕ. Integrating (3.1) over a small cuboidal cell of volume $\mathrm{d}V$ yields

$$\int_V \frac{\partial \rho\phi}{\partial t}\,\mathrm{d}V = \bar{S}_\phi + \sum_{x,y,z}\left[\left(\Gamma_\phi \frac{\partial \phi}{\partial x_k} - \rho u_k \phi\right) A\right]_-^+,$$

where $\bar{S}_\phi$ is the volume integral of the source term and the term in square brackets represents the surface integral over the cell face area, A, of the convective and diffusive fluxes across each face of the cuboid. It is necessary to find a numerical approximation to each of the convective and diffusive flux terms, and this is done with the aid of a simple staggered grid arrangement. All scalar quantities are assumed to be stored at cell centres, while each velocity component is assumed to be stored at the centre of the appropriate cell face. Using central differencing and local averaging between adjacent points, a uniformly second-order accurate scheme is generated that uses only nearest-neighbour points, and, hence, is ideally suited to a parallel domain-decomposition strategy. Evaluation of the source term $\bar{S}_\phi$ is straightforward, since second-order accuracy is achieved simply by setting $\bar{S}_\phi = S_\phi V$.

Temporal discretization makes use of the explicit second-order Adams–Bashforth method coupled to a velocity projection algorithm described by Gavrilakis *et al.* (1985). The general form of the spatially discretized conservation equations is now

$$\frac{\partial}{\partial t}(\overline{\rho\phi})V = \bar{S}_\phi + H(\phi),$$

where $H(\phi)$ contains the discretized convective and diffusive fluxes. According to the Adams–Bashforth scheme this becomes

$$[(\overline{\rho\phi})^{n+1} - (\overline{\rho\phi})^n]\frac{V}{\delta t} = \tfrac{3}{2}(H^n(\phi) + \bar{S}_\phi^n) - \tfrac{1}{2}(H^{n-1}(\phi) + \bar{S}_\phi^{n-1}),$$

where the superscripts indicate the time level at which each term is evaluated. A single explicit step is sufficient for time advancement of the scalar variables, but time advancement of the velocity components also requires the satisfaction of the continuity constraint. This is achieved by projecting the velocity components, u, v, w, to an intermediate pseudo-time level. Dropping the overbars for clarity, the equation for the u velocity component may be written

$$[(\rho u)^* - (\rho u)^n]\frac{V}{\delta t} = \tfrac{3}{2}(H^n(u) + \hat{S}_u^n) - \tfrac{1}{2}(H^{n-1}(u) + S_u^{n-1}),$$

where the modified source term, $\hat{S}_u^n$, does not include the pressure gradient contribution, i.e.

$$\hat{S}_u^n = S_u^n - (\nabla_x P)^n V,$$

where the pressure gradient term is given by

$$\nabla_x P = \frac{P_{i+1,j,k} - P_{i,j,k}}{\delta x}.$$

Expressions for the v and w components follow in the obvious manner. The time advancement of the u velocity component is completed using

$$[(\rho u)^{n+1} - (\rho u)^*]\frac{V}{\delta t} = -\tfrac{3}{2}(\nabla_x P)^n V,$$

where the pressure has been computed from the discrete Poisson equation

$$(\nabla^2 P)^n = \frac{2}{3}\frac{1}{\delta t}(\operatorname{div} M^* - \operatorname{div} M^{n+1}), \tag{3.2}$$

in which $\operatorname{div} M$ is the discrete mass flux divergence across the computational cell. This is a classical projection method, and, despite the operator-splitting step, the overall method may be shown to be second-order accurate in time.

Note that, in the case of constant-density flow, the mass flux divergence at each true time level is identically zero, whereas the mass flux divergence at the pseudo-time level in general is non-zero, since continuity has not been enforced. For combustion problems involving heat release, the mass flux divergence is generally non-zero even at real time levels due to thermal expansion. This is accounted for by using the full continuity equation in the form

$$(\rho^{n+1} - \rho^n)\frac{V}{\delta t} + \tfrac{1}{2}(\operatorname{div} M^{n+1} + \operatorname{div} M^n) = 0,$$

which corresponds to a second-order Crank–Nicholson discretization in time. Substituting this equation into (3.2) yields the full variable-density form of the pressure Poisson equation:

$$(\nabla^2 P)^n = \frac{2}{3}\frac{1}{\delta t}\left(\operatorname{div} M^* + \operatorname{div} M^n + 2(\rho^{n+1} - \rho^n)\frac{V}{\delta t}\right).$$

The discrete Poisson equation for the pressure has a particularly simple form on a uniform staggered grid and may be solved very efficiently using standard techniques, such as Fourier or conjugate gradient methods.

It is well known that the second-order Adams–Bashforth scheme is weakly unstable for pure convection problems, but the strongly diffusive nature of the present class of flame-propagation problems provides more than adequate damping, without loss of second-order accuracy. Stability analysis, together with heuristic testing, has shown that the behaviour of the present method is governed by classical Courant and diffusive stability relations.

4. Test problems

A computer code called Angus has been written to solve the governing equations using the numerical methods outlined above. The code is written in Fortran 77 and has been ported to many different workstation computers running the Unix operating system. Parallel extensions to the code were implemented using PVM and Cray *shmem* library calls by Dr D. R. Emerson at Daresbury Laboratories, and the parallel version has been run on several distributed-memory architectures. The principal effort has been directed towards the Cray T3D and T3E machines at Edinburgh Parallel Computer Centre and the code has been highly optimized for these systems. The Poisson equation for pressure is solved using a parallel conjugate gradient method with optional MILU preconditioning, and performance in parallel has proved to be very satisfactory.

The code has been used for a number of investigations of turbulent premixed flame propagation. In each case, a field of homogeneous isotropic turbulence is generated using random Fourier modes satisfying the continuity equation and a specified initial energy spectrum $E(k)$. A spectrum function used by Lee & Reynolds (1985) is chosen in the form

$$E(k) = \begin{cases} \gamma_{\mathrm{E}} k^2, & \text{for } k_{\min} \leqslant k \leqslant k_{\mathrm{peak}}, \\ \gamma_{\mathrm{E}} k_{\mathrm{peak}}^2 (k/k_{\mathrm{peak}})^{-5/3}, & \text{for } k_{\mathrm{peak}} < k \leqslant k_{\max}, \\ 0, & \text{otherwise.} \end{cases} \tag{4.1}$$

The three velocity components are obtained by performing an inverse Fourier transform to physical space. While continuity is satisfied accurately within each finite-difference cell, the property of isotropy is satisfied in a statistical sense only, and some care is required given the limited sample size of large-scale eddies. The initial field has realistic second-moment statistics but higher moment properties must be allowed to develop. This is achieved by running the code for a short time to allow the turbulence to become established. The governing Reynolds number of the simulation is $Re = \rho_0 u_0 l_0/\mu_0$, where l_0 is the size of the box, and its value must be chosen with care to allow adequate resolution of the smallest scales of motion. A value of $Re \simeq 50$

has proved adequate for a box size of 128^3 points. Tests have been carried out to check the properties of the non-reacting turbulent field by running simulations of decaying isotropic turbulence in a cubic domain with periodic boundary conditions. Results have demonstrated that the representation of the turbulence is accurate in terms of isotropy and spectral correlations, and that the decay of turbulent kinetic energy is well captured.

Reacting simulations require an initial flame to be specified. This is done by means of a series of one-dimensional calculations of constant-density premixed laminar flames, in which the parameters controlling the reaction rate (i.e. B^*, β and α) are varied, with the Reynolds number held fixed at the value required for the turbulent simulation. A laminar-flame solution is selected having a normalized burning velocity close to unity and a well-resolved reaction zone structure. Two flames are produced, oriented back-to-back in order to preserve the periodicity of the boundary conditions. The chosen back-to-back flame solution is extended to three dimensions as a pair of planar flames and is introduced into the established turbulent simulation straddling the central x-plane of the domain.

For parallel processing, a simple domain-decomposition strategy is followed. The entire computational domain is decomposed by assigning a spatially contiguous sub-domain to each processor. The mapping between sub-domains and processors is a straightforward x–y–z ordering, kept precisely the same as that used to designate points within the computational grid. Load balancing between processors demands that all sub-domains be of equal size, although unequal sub-domains may be accommodated at some penalty in parallel efficiency. Each sub-domain overlaps its neighbours by one cell, forming a 'halo' of data that must be passed from each processor to the next in each direction at each update. For scalar variables the transfer takes place once per time-step, for velocity components twice per time-step, and for pressure there are as many transfers as iterations within the Poisson equation solver.

The simulation proceeds with the flames responding to the turbulent environment and becoming wrinkled and curved in three dimensions. The simulation is ended when one or both flames is/are about to propagate out of the domain, or when the turbulence has decayed to a point where the integral length-scale is becoming comparable with the size of the domain.

5. Results

Results from four simulation runs are presented. The grid size was fixed at 128^3 points and the four runs are specified according to the magnitude of the initial turbulence intensity u'/u_l, which was set to 1.0, 2.0, 5.0 and 10.0 in runs 1–4, respectively. The nominal Reynolds number was set to 30 and the Prandtl number to 0.7. The Lewis number was fixed at unity for this series of runs, and the temperature equation (2.15) was dropped. A field of homogeneous isotropic turbulence was generated from the initial spectrum function with parameters $k_{\min} = 1.0$, $k_{\text{peak}} = 10.0$ and $k_{\max} = 60.0$, and with γ_{E} set to match the required total energy for each run, taking values of 4.3857×10^{-6}, 1.7543×10^{-5}, 1.0964×10^{-4} and 4.3857×10^{-4}, respectively, in runs 1–4.

A laminar-flame profile was also computed with parameters $B^* = 480.0$, $\beta = 6.0$ and $\alpha = 0.75$, to yield a non-dimensional flame speed of unity. The heat release implied by this fairly modest value of α was not fed back to the flow field and

Table 1. *Principal flow field statistics at the end of each run, at non-dimensional time* $t/\tau = 0.15$

run number	1	2	3	4
$u'/u_l\|_{t=0}$	1.0	2.0	5.0	10.0
k/u_l^2 $(\times 10^{-3})$	1.762	6.932	40.61	141.3
$\varepsilon \times \tau/u_l^2$ $(\times 10^{-2})$	1.993	7.883	46.78	164.8
mass fraction burned	0.283	0.283	0.287	0.298
Kolmogorov length l_k/L	0.208	0.147	0.094	0.069
Taylor length λ/L	0.169	0.168	0.167	0.167
integral length l_{T}/L	0.450	0.444	0.451	0.460

the density remained constant throughout. Each simulation was distributed over 64 nodes of the T3D machine and was run initially for 100 time-steps (non-dimensional time $t/\tau = 0.01$) without reaction to allow the turbulence to evolve. At this time, the back-to-back laminar-flame solution was introduced and the simulation was continued. A dataset was obtained at each subsequent 100 time-steps containing the entire velocity field together with the reaction-progress variable field, each dataset occupying *ca.* 85 Mb of disk space. Each simulation was run for a total of 1500 time-steps, with each run requiring a total of *ca.* 15 hours of CPU time on the 64 processors. The datasets were archived to tape for subsequent post-processing. Table 1 shows a summary of the flow field statistics obtained after completion of the run. The flame has consumed almost 30% of the mass and combustion is somewhat further advanced in the high-turbulence cases. The turbulence kinetic energy has decayed very substantially and the dissipation rates remain in step. Integral length-scales obtained by direct correlation show that the large-scale eddies are occupying almost half of the box, so that the decision to stop the simulation is timely on turbulence grounds. The Kolmogorov scale is well resolved for all cases with more than eight cells in a Kolmogorov eddy at all times. Only directionally averaged statistics are shown, but the Taylor and integral scales do display some evidence of anisotropy due to the small sample of large scales present in the initial field.

It is evident from the table that the flow in the lowest turbulence case (run 1) is almost laminar, and that run 4, having the highest turbulence, should display the greatest degree of flame wrinkling. This is clear from figure 1, which shows the velocity vectors and reaction-progress variable contours from the lower-left octant of the domain, on the plane $z = 0$ at time $t/\tau = 0.15$. The flame shows progressively greater wrinkling with increased turbulence intensity. Time histories of flame propagation (not shown here) demonstrate that small-scale wrinkling is imposed by the turbulence on the flame at early times but does not persist and is removed by the smoothing effect of flame propagation.

A principal aim of the present study is to collect statistical data on the response of the flame surface to turbulent straining and curvature. To this end, probability density function (PDF) data have been obtained for quantities of interest in turbulent-combustion modelling. The first step in the surface-data collection procedure is to locate the flame surface. This is accomplished by interpolating the reaction-progress variable c along each x-line of the grid. Cubic spline interpolation is found to be appropriate in that it combines second-order accuracy with second-derivative con-

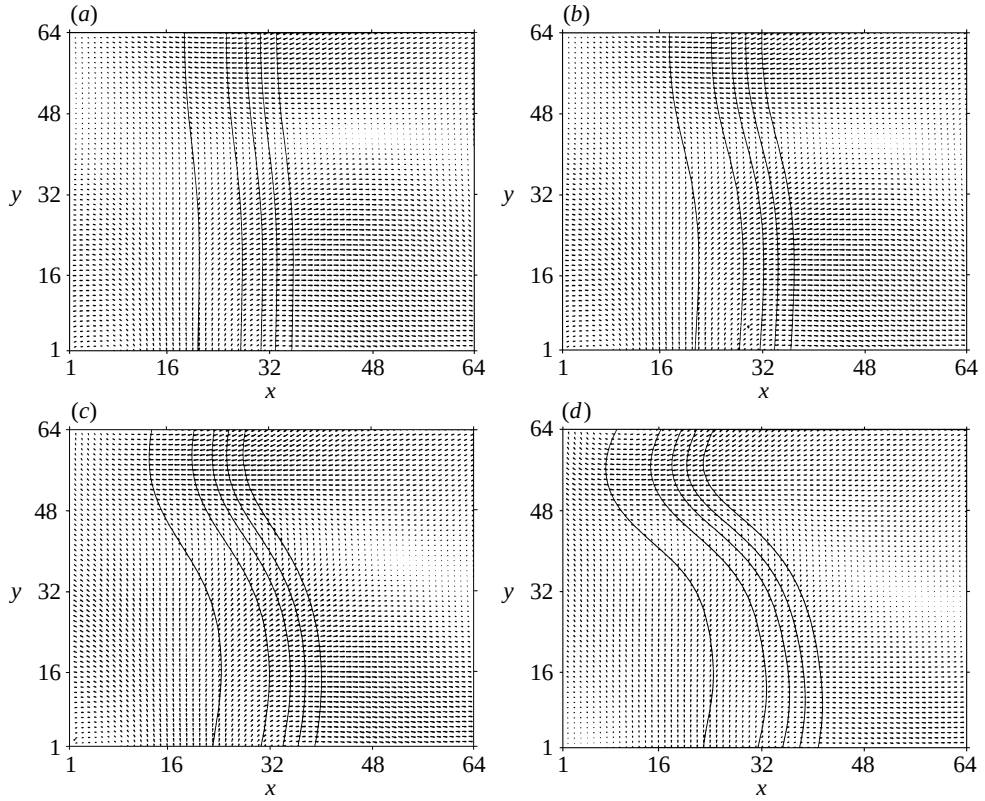

Figure 1. Velocity vectors and contours of the reaction-progress variable at the end of each run, at non-dimensional time $t/\tau = 0.15$. A single plane ($z = 0$) is shown, in the left front octant of the domain: (*a*) run 1 (lowest turbulence); (*b*) run 2; (*c*) run 3; (*d*) run 4 (highest turbulence).

tinuity. The spatial position x_f corresponding to a fixed value c_f of the progress variable does not, in general, coincide with a grid point and is found using a bisection method on the interpolating function. At least two flame locations are expected on each x-line, since the domain contains two flames oriented back-to-back in the x-direction. Multiple intersections are possible in principle, but it is interesting to note that the geometry constrains the total number of flame intersections on each x-line to be even.

The first physical quantity of interest is the flame surface normal vector $\boldsymbol{N}$, defined on the basis of the progress variable gradient and oriented so as to point in the direction of flame propagation, i.e.

$$\boldsymbol{N} = -\frac{\nabla c}{|\nabla c|}.$$

The components of the progress variable gradient are evaluated at each grid point, using a numerical approximation to the spatial derivative that is consistent with the scheme used in the Angus code. The components are then interpolated onto the flame surface location $x_\mathrm{f} = x(c = c_\mathrm{f})$ and the normal vector is evaluated. This is repeated for each surface point and a probability density function (PDF) is constructed using a standard frequency-table method. Given two flames and the size of

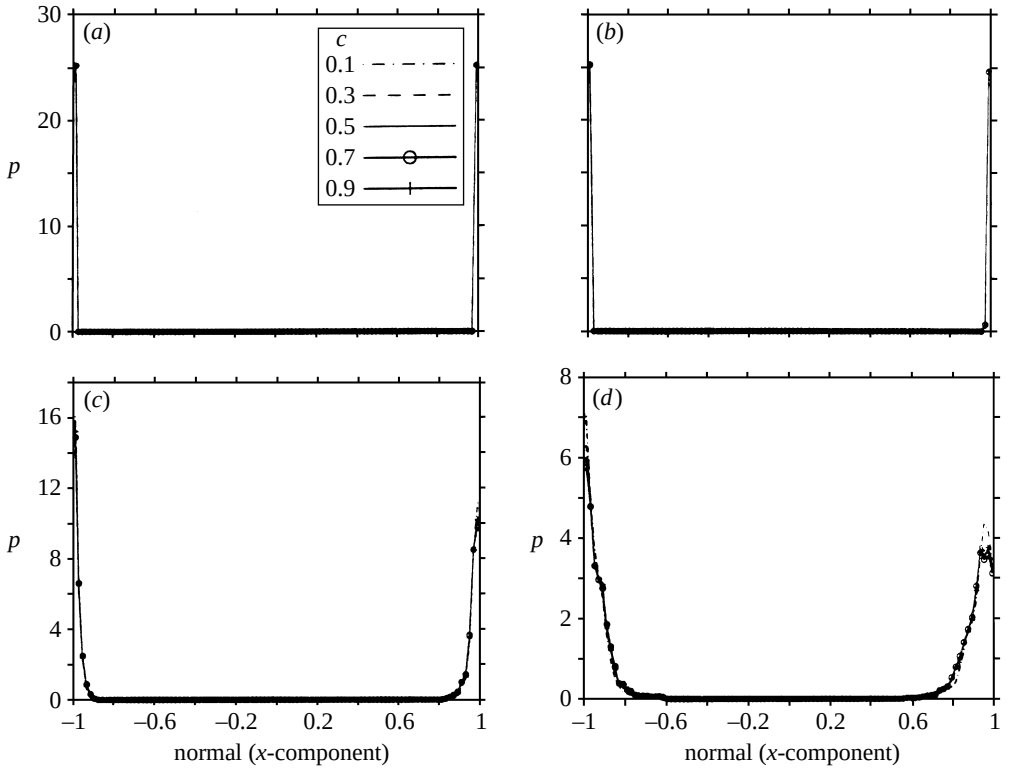

Figure 2. Probability density function of the x-component of the flame surface normal, taken at $t/\tau = 0.15$ for each of the four runs: (*a*) run 1; (*b*) run 2; (*c*) run 3; (*d*) run 4.

the domain, the sample size is at least 2×128^2. Figure 2 shows the PDFs obtained for the x component of the flame normal in the highest turbulence case, at $t/\tau = 0.15$, i.e. towards the end of the run. Different line styles indicate different choices of progress variable location within the flame, ranging through $c_\mathrm{f} = 0.1$, 0.3, 0.5, 0.7 and 0.9, but it is clear that there is no significant variation of the local normal in passing through the flame. The two peaks in the PDF correspond to the left- and right-propagating flames, and show that each flame surface is broadly oriented in its own direction of propagation. The peaks do broaden as turbulence intensity is increased, but there is a low probability of significant deviation from the mean direction of propagation, and the mean of the x component does not fall below a value of 0.923, even for the highest turbulence case.

The tangential strain rate a_T, taken locally in the plane of the flame, is a quantity of considerable interest in modelling due to its importance in affecting the local rate of propagation in a turbulent flame. The strain-rate tensor,

$$s_{ij} = \frac{1}{2}\left(\frac{\partial u_i}{\partial x_j} + \frac{\partial u_j}{\partial x_i}\right),$$

is computed at each grid point, and the tensor is then interpolated onto the flame surface location x_f. The tensor is then rotated into a coordinate system aligned with the local flame surface normal, and the tangential strain rate a_T is given by the sum

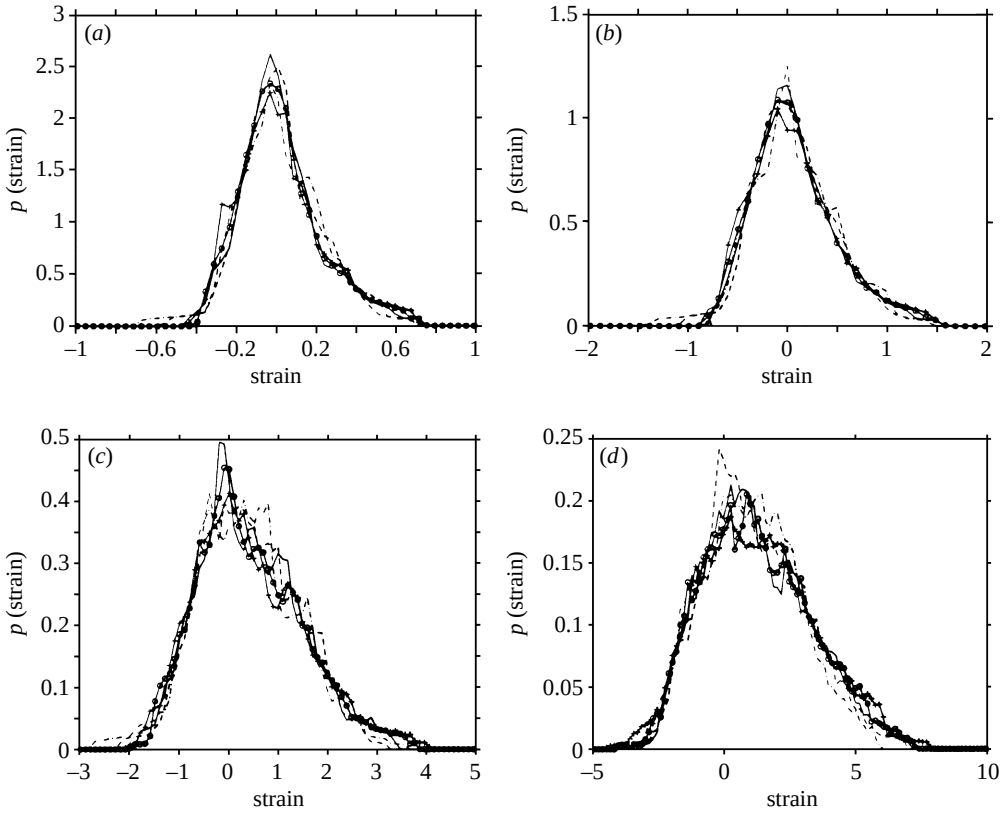

Figure 3. Probability density function (PDF) of the tangential strain rate in the plane of the flame surface, taken at $t/\tau = 0.15$ for each of the four runs: (*a*) run 1; (*b*) run 2; (*c*) run 3; (*d*) run 4.

of the strain-rate eigenvalues in the plane tangent to the flame. This procedure is repeated at all flame surface points on both flames and a PDF is assembled. Results are shown in figure 3 for the four runs. It is clear that the shape of the PDF is similar for all runs, having a slight asymmetry that tends to favour positive values. The mean is slightly positive in all cases and increases strongly with increasing turbulence intensity, while the width of the distribution also increases with u'/u_l. This is consistent with the traditional picture of turbulence acting to stretch an embedded surface, but the distributions also show a significant probability of negative straining or compression of the flame.

The curvature of the flame surface may be treated in a similar manner. The gradients of the flame surface normal are evaluated and used to form a tensor $\partial N_i/\partial x_j$ at each flame surface point x_f. This tensor is rotated into a coordinate system aligned with the flame normal, and the two principal curvatures of the flame surface, h_1 and h_2, are obtained as eigenvalues in the tangent plane. The sign convention is that positive curvature is defined as convex towards reactants. The mean curvature $h_\mathrm{m} = 1/2(h_1 + h_2)$ is evaluated and PDFs are shown in figure 4 for each of the four runs. It is clear that there is a considerable spread of the PDFs according to location within the flame. At the front of the flame, the tendency is towards higher proba-

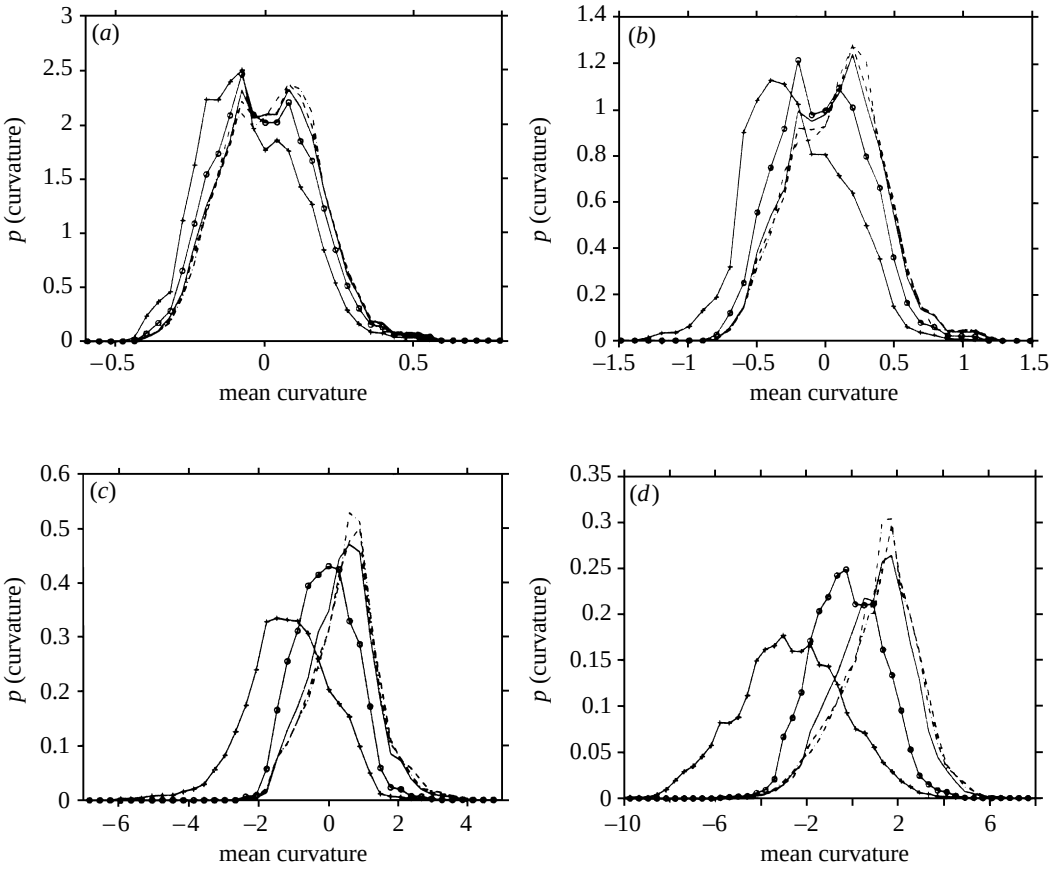

Figure 4. Probability density function of the mean curvature of the flame surface, taken at $t/\tau = 0.15$ for each of the four runs: (*a*) run 1; (*b*) run 2; (*c*) run 3; (*d*) run 4.

bility for positive curvature, that is for the flame to curve in a sense convex towards the reactants. Conversely, at the rear of the flame the tendency is towards higher probability for curvature in the opposite sense, that is concave towards the reactants. This observation can be explained with reference to Huygens's principle, whereby the propagation of a symmetric initial perturbation will cause it to grow preferentially in the direction of mean propagation. Parts of the flame that are perturbed in a convex sense will become larger and more gently curved, while parts of the flame that are initially concave will become smaller and more tightly curved. Thus the magnitude of the curvature will tend to be larger in negatively curved regions and smaller in positively curved regions of the flame. The strong dependence on location within the flame is a consequence of the finite thickness of the flame, which acts to magnify the Huygens effect.

Assembling the joint PDF of tangential strain rate and mean curvature is straightforward given the data already computed on surface points. Contour plots of the joint PDF are shown in figure 5 for the highest turbulence case (run 4) for five different values of progress variable location c_{f}. The joint PDF appears to be well described

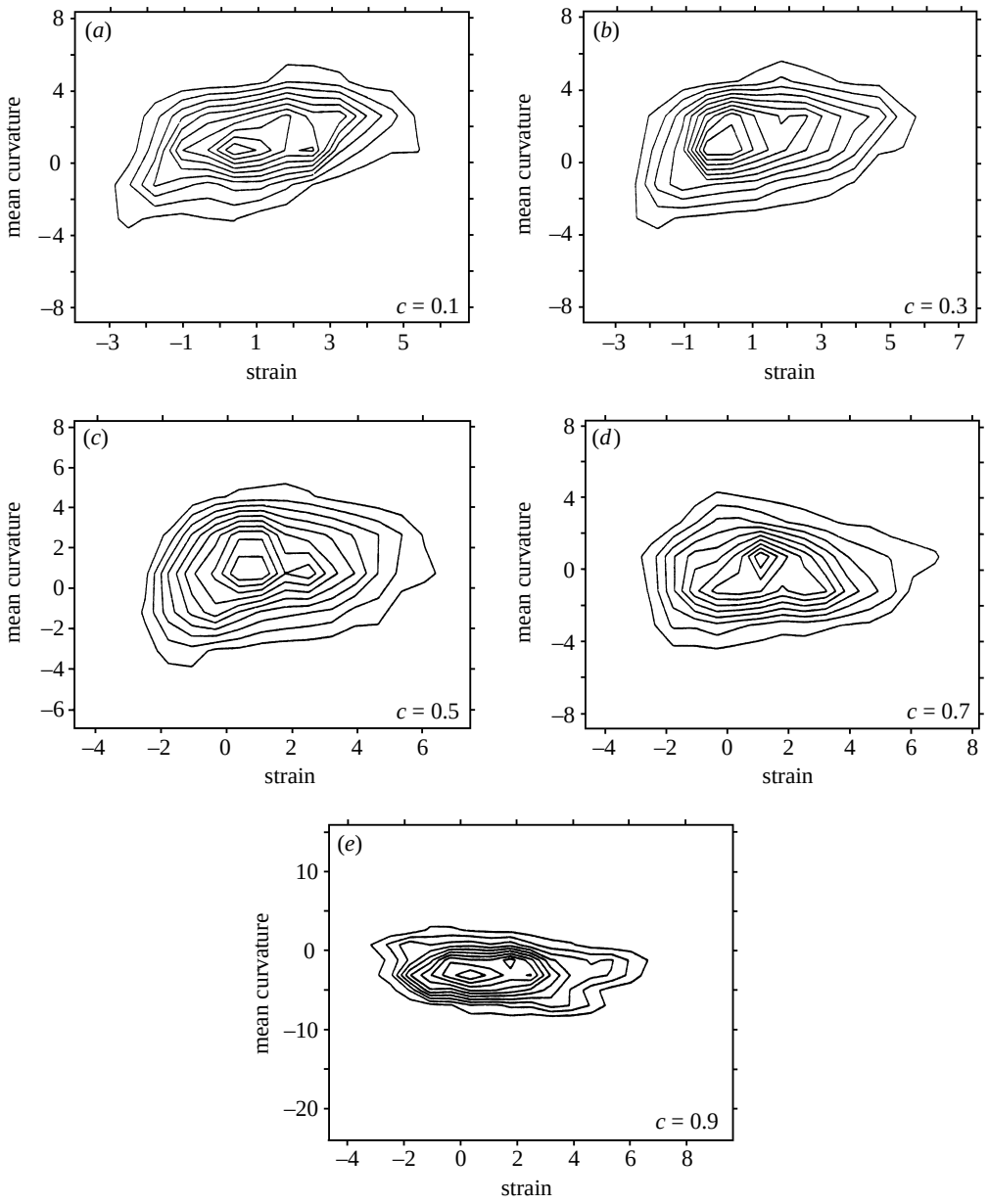

Figure 5. Joint probability density function of the tangential strain rate (x-axis) and mean curvature (y-axis) taken at $t/\tau = 0.15$ at five different locations within the flame. (a) $c = 0.1$; (b) $c = 0.3$; (c) $c = 0.5$; (d) $c = 0.7$; (e) $c = 0.9$.

by the product of the marginal PDFs, and very little correlation between strain and curvature is apparent. There is little variation with location through the flame. The lack of correlation is interesting, since it appears that there is no statistical connection between strain and curvature effects, at least on an instantaneous and local basis. For modelling purposes, the implication is that strain and curvature effects

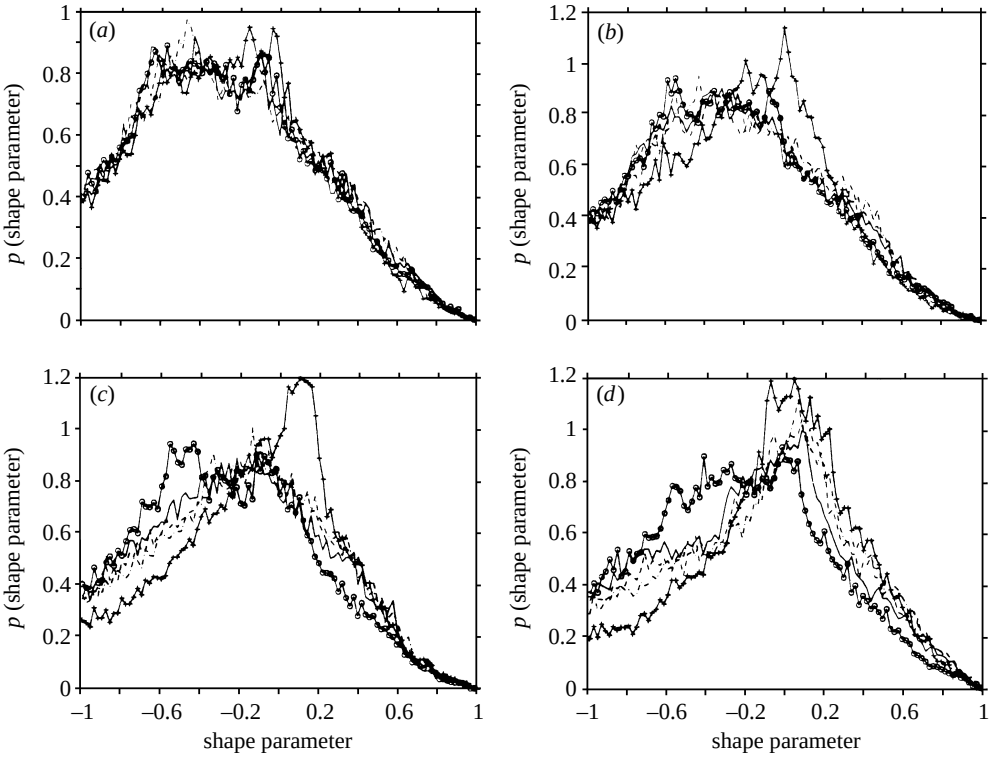

Figure 6. Probability density function of the curvature shape factor taken at $t/\tau = 0.15$ for each of the four runs: (*a*) run 1; (*b*) run 2; (*c*) run 3; (*d*) run 4.

can be treated separately. A cautionary note is that the Lewis number is unity in the present case and a correlation has been observed in simulations of non-unity Lewis number flames (Rutland & Trouve 1993).

Information on the flame shape may be obtained by computing the curvature shape parameter s_h, defined as the smaller of the two principal curvatures by magnitude divided by the other (Pope *et al.* 1989). This quantity takes the value zero for spheres, unity for cylinders and -1 for spherical saddle points. PDFs for the curvature shape factor are shown in figure 6 for the four runs. Immediate conclusions for all runs are that spherical shapes do not appear on the flame at all and that cylindrical curvature is dominant. Spherical saddle points occur with modest probability. There is little spread in the results through the flame. The precise mechanism behind this outcome is not clear, but it seems likely that the flame is never curved by the turbulence with equal magnitudes in the two principal directions. The effect of propagation is then to reduce the curvature magnitude for convex curvature and to increase it for concave curvature. Thus there is no tendency towards equality of curvature magnitude if both of the initial curvatures are of the same sign. Only in the case where the initial curvatures are of opposite sign does the possibility exist that a spherical saddle point will evolve through propagation. Once again, the implication for modelling is favourable, in that only one of the two curvatures appears to be important at each surface location.

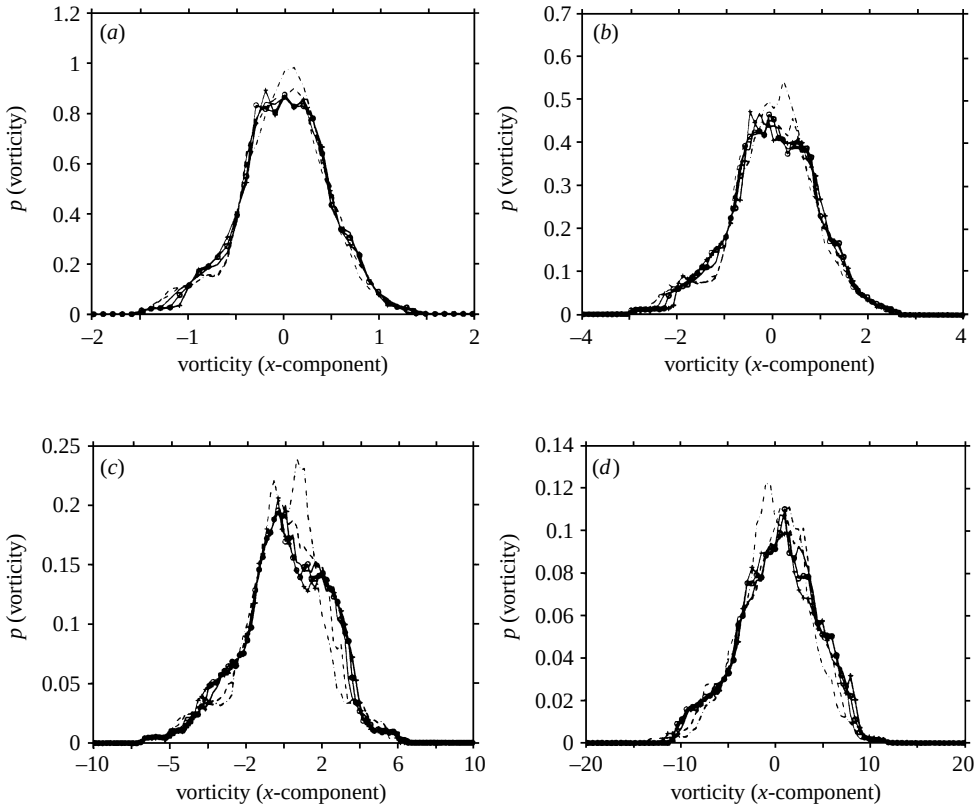

Figure 7. Probability density function of the x-component of the vorticity on the flame surface taken at $t/\tau = 0.15$ for each of the four runs: (a) run 1; (b) run 2; (c) run 3; (d) run 4.

The cylindrical curvature of the flame surface suggests that the presence of vortices in the turbulent-flow field may play some role in the flame–turbulence interaction process. This was investigated by evaluating the components of the vorticity vector $\omega_i = \nabla \times \boldsymbol{u}$ on the flame surface. This was done in the same manner as for the strain-rate tensor, and the surface PDF of vorticity components was produced in the same way. Results are shown in figure 7 for the x-component of vorticity and show a central distribution with zero mean and a variance increasing with turbulence intensity. The y and z components show statistically identical results, demonstrating that the vorticity on the flame surface is isotropic. Thus there is no evidence of preferential alignment of vortices either parallel or perpendicular to the flame, at least on the basis of results local to the flame surface.

There remains the possibility that the flame may be influenced by a vortex whose core is at some distance from the flame surface. Direct statistical evidence for this would require a two-point analysis, which is outside the scope of the present investigation. Nevertheless, some circumstantial evidence for vortical action at a distance may be found by examining the interaction between strain and curvature. The hypothesis is that the local cylindrical curvature of the flame is due to the influence of a vortex lying parallel to the flame surface but at some distance away. The flame will then feel

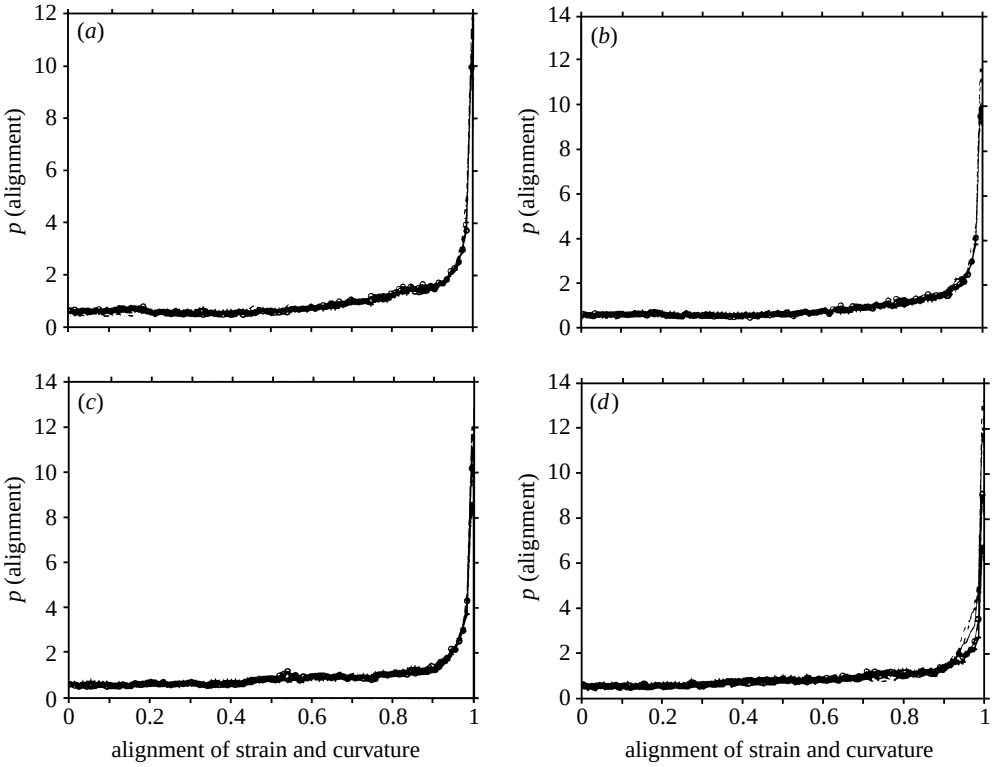

Figure 8. Probability density function of the scalar product $\boldsymbol{s}_1 \cdot \boldsymbol{h}_2$ on the flame surface, taken at $t/\tau = 0.15$ for each of the four runs: (*a*) run 1; (*b*) run 2; (*c*) run 3; (*d*) run 4.

the effect of the strain field that acts to stretch the vortex along its length according to the well-known turbulent vortex-stretching mechanism. In that case, the strain-rate eigenvector $\boldsymbol{s}_1$ associated with the larger of the two strain-rate eigenvalues in the flame surface will align preferentially with the curvature eigenvector $\boldsymbol{h}_2$ associated with the smaller of the two curvature eigenvalues. In other words, the flame will be strained preferentially along the axis of its own cylindrical curvature. The relevant eigenvalues and eigenvectors have already been computed as part of the evaluation of strain-rate and curvature PDFs, and it is straightforward to calculate the scalar product $\boldsymbol{s}_1 \cdot \boldsymbol{h}_2$ and to assemble its PDF in the flame surface. Results for this PDF are shown in figure 8 for each of the four runs. In all cases, the PDF shows a strong peak at a scalar product value of unity, which indicates that these vectors do indeed tend to align. The conclusion is that the observed cylindrical curvature of the flame surface is due, at least in part, to the tendency of the flame to be drawn into the strain field of nearby vortices.

6. Conclusions

Direct numerical simulations have been carried out to investigate the interaction of a premixed flame with a turbulent field. A general formulation has been presented and necessary simplifications have been carried out in order to render the problem

tractable on present-day computers. Emphasis has been given to the need for numerical methods suitable for use on massively parallel computers and an example of one such approach has been outlined. Results have been presented for four simulations carried out at different initial turbulence intensities. Quantities such as strain rates and curvatures local to the flame surface are of considerable value in modelling and have been obtained from the DNS results in a straightforward manner. Some useful observations have been made concerning the statistical geometry of the flame surface, and evidence has been gathered concerning a possible kinematic explanation for the curvature of the flame.

A great deal of work remains to be done in both formulating and using DNS in support of modelling efforts. It is generally agreed that second-order numerical schemes represent the minimum acceptable accuracy for DNS and it is desirable to move on to the use of higher-order methods. This will represent a considerable challenge to designers of parallel algorithms. It is necessary to carry out many more simulations in order to build up a picture of the variations of the quantities of interest, such as strain rates and flame curvatures, with changes in turbulence intensities, length-scales and parameters such as Lewis number. It is also necessary to address the problems of including realistic chemical reaction mechanisms in three-dimensional DNS, so that, in due course, the simulations may be truly direct in all aspects.

Financial support and computing resources for this work were provided by the EPSRC. Parallel computing support from Dr D. R. Emerson and technical contributions from Dr W. K. Bushe and Dr L. L. Leboucher have been essential and are gratefully acknowledged.

Nomenclature

A	area
A_m	frequency factor for reaction step m
a_{T}	tangential strain rate
a_0	speed of sound in reactants
B	pre-exponential factor
B^*	non-dimensional pre-exponential factor
C_V, C_P	specific heat capacities
c	reaction-progress variable
D	diffusivity of progress variable
E	activation energy for progress variable
$E(k)$	turbulence energy spectrum function
E_m	activation energy for reaction step m
H	heat of reaction per unit mass of reactants
$H(\phi)$	convective and diffusive operator
h_{m}	mean curvature of flame surface
$\boldsymbol{h}_2$	eigenvector associated with second principal curvature
h_α	enthalpy of species α
k	wavenumber
$\mathcal{M}$	Mach number
M	number of reaction steps
$\mathrm{div}\, M$	mass flux divergence

N	number of species α in the mixture
$\boldsymbol{N}$	flame normal vector
n_m	temperature exponent for reaction step m
P	pressure
Pr	Prandtl number
q_i	heat flux vector
R_0	universal gas constant
Re	Reynolds number
S	source term
Sc	Schmidt number
s_h	curvature shape factor
s_{ij}	strain-rate tensor
$\boldsymbol{s}_1$	eigenvector associated with first principal strain rate
T	temperature
t	time
u'	turbulence intensity
u_i (also u, v, w)	velocity components
u_l	laminar-flame speed
V	volume
$V_{\alpha i}$	diffusion velocity of species α
W_α	molar mass of species α
w_α	reaction rate of species α
x_i (also x, y, z)	spatial coordinates
Y_α	mass fraction of species α
α	heat release parameter
β	Zeldovich number
Γ	general diffusivity
γ	specific heats ratio
γ_{E}	parameter in energy spectrum function
ε	turbulence energy dissipation rate
λ	thermal conductivity
μ	viscosity
$\nu'_{\alpha,m}, \nu''_{\alpha,m}$	stoichiometric coefficients
ρ	density
τ	laminar-flame passage time
τ_{H}	heat release parameter
τ_{ij}	viscous stress tensor
ϕ	general quantity
ω_i	vorticity

References

Alshaalan, T. M. & Rutland, C. J. 1998 Turbulence, scalar transport and reaction rates in flame–wall interaction. In *Proc. 27th Symp. (Int.) on Combustion*, pp. 793–799. The Combustion Institute.

Baum, M., Poinsot, T. J. & Thevenin, D. 1998 Accurate boundary conditions for turbulent reactive flows. *J. Comput. Phys.* **116**, 247–261.

Bray, K. N. C. & Cant, R. S. 1991 Some applications of Kolmogorov's turbulence research in the field of combustion. *Proc. R. Soc. Lond.* A **434**, 217–240.

Bushe, W. K. & Cant, R. S. 1996 Results of direct numerical simulations of turbulent premixed combustion. Report CUED/A-THERMO/TR63. Cambridge University Engineering Department.

Bushe, W. K., Leboucher, L. L. & Cant, R. S. 1997 Parallel direct numerical simulation of turbulent flames. In *Parallel CFD '97, Manchester*.

Cant, R. S., Rutland, C. J. & Trouve, A. 1990 Statistics for laminar flamelet modeling. In *Proc. 1990 Summer Program, Center for Turbulence Research, Stanford, CA*, pp. 271–279.

Echekki, T. & Chen, J. H. 1996 Unsteady strain rate and curvature effects in turbulent premixed methane–air flames. *Combust. Flame* **106**, 184–202.

Gavrilakis, S., Tsai, H. M., Voke, P. R. & Leslie, D. C. 1985 Large-eddy simulation of low Reynolds number channel flow by spectral and finite difference methods. In *Proc. Euromech. Coll.*, no. 199, pp. 105–118. Braunschweig: Vieweg.

Harlow, F. H. & Welch, J. E. 1965 Numerical calculation of time-dependent viscous incompressible flow of fluid with free surface. *Phys. Fluids* **8**, 2182–2185.

Kollman, W. & Chen, J. H. 1998 Pocket formation and the flame surface density equation. In *Proc. 27th Symp. (Int.) on Combustion*, pp. 927–934. The Combustion Institute.

Lee, M. J. & Reynolds, W. C. 1985 Numerical experiments on the structure of homogeneous turbulence. Technical Report TF-24, Thermosciences Division, Department of Mechanical Engineering, Stanford University, CA.

Lele, S. K. 1992 Compact finite difference schemes with spectral-like resolution. *J. Comput. Phys.* **103**, 16–42.

Orszag, S. A. 1969 Numerical methods for the simulation of turbulence. *Phys. Fluids* (Suppl. 2) **12**, 250–257.

Poinsot, T. J. & Lele, S. K. 1992 Boundary conditions for direct numerical simulations of compressible viscous flows. *J. Comput. Phys.* **101**, 104–129.

Poinsot, T. J., Candel, S. & Trouve, A. 1995 Direct numerical simulation of premixed turbulent combustion. *Prog. Energy Combust. Sci.* **21**, 531–576.

Pope, S. B., Yeung, P. K. & Girimaji, S. S. 1989 The curvature of material surfaces in turbulence. *Phys. Fluids* A **1**, 2010–2018.

Riley, J. J., Metcalfe, R. W. & Orszag, S. A. 1986 Direct numerical simulation of chemically reacting turbulent mixing layers. *Phys. Fluids* **29**, 406–422.

Rutland, C. J. & Cant, R. S. 1994 Turbulent transport in premixed flames. In *Proc. 1994 Summer Program, Center for Turbulence Research, Stanford, CA*, pp. 75–94.

Rutland, C. J. & Trouve, A. 1993 Direct simulations of premixed turbulent flames with nonunity Lewis numbers. *Combust. Flame* **94**, 41–57.

Rutland, C. J., Ferziger, J. H. & El-Tahry, S. H. 1990 Full numerical simulations and modeling of turbulent premixed flames. In *Proc. 23rd Symp. (Int.) on Combustion*, pp. 621–627. The Combustion Institute.

Vervisch, L. & Poinsot, T. J. 1998 Direct numerical simulation of non-premixed turbulent flames. *A. Rev. Fluid Mech.* **30**, 655–691.

Zhang, S. & Rutland, C. J. 1995 Pressure effects in turbulent transport of premixed flames. *Combust. Flame* **102**, 447–461.